This manuscript has been published by the Engineering Structure 2019, Vol. 201, pp.109849.
doi.org/10.1016/j.engstruct.2019.109849

Behaviour of H-section purlin connections in resisting progressive collapse of roofs

Shen Yan[1,2], Kim J.R. Rasmussen[2], Xinlu Liu[1], Liusi Dai[3], Xianzhong Zhao[1]

1. College of Civil Engineering, Tongji University, China
2. School of Civil Engineering, the University of Sydney, Australia
3. School of Civil Engineering, Shanghai University, China

Abstract:

When a truss roof is subjected to sudden local damage, purlins are capable of bridging the damaged planar truss unit, thereby increasing the robustness of the integrated roof system. To investigate the bridging capacity that purlins can provide, experiments were carried out on the bolted fin plate connections that join thin-walled H-section purlins to the main truss, investigating their behaviour under a main truss-removal scenario. Eight specimens with varied connection details were tested. Results of all experiments are provided in detail, including the full-range vertical resistance-displacement curves, the collapse-resisting mechanisms, and the failure modes, being either bolt shear failure or combined bolt bearing and net-section tensile failure. Meanwhile, a theoretical model is proposed to predict the vertical resistance-displacement response of the purlin-to-connection assembly. This model is capable of capturing the slip of bolts, and the gradual yielding and failure of the connection components, and thus gives predictions that are in reasonably good agreement with the experimental results.

Keywords:

progressive collapse; purlin connection; experiments; bolt slip; component model

This manuscript has been published by the Engineering Structure 2019, Vol. 201, pp.109849.
doi.org/10.1016/j.engstruct.2019.109849

1. Introduction

The last several decades have witnessed plenty of progressive collapse incidents of building structures, leading to a growing interest in both the academic and engineering communities in this disproportional failure phenomenon. As a result, a great number of studies have been conducted to investigate the progressive collapse resistance of multi-storey frame structures [1-3] and, more recently, roof structures [4-6].

Among the various types of roof structures, trusses have received the most attention in the research of progressive collapse. It is already known that a planar truss unit has two mechanisms for stopping the spread of the initial damage inside the planar truss unit, i.e., arch action and catenary action [7-9]. When multiple planar truss units are tied into an integrated roof system, the tying members such as purlins are capable of bridging the initially damaged truss unit [10]. This is readily understandable because a good analogy can be found in frame structures, in which the catenary behaviour of beams bridges the initially damaged column. However, what remains unknown is the actual bridging capacity a purlin can provide, which primarily relies on the resistance and ductility of the purlin-to-main truss connection.

Compared to thin-walled C-shaped and Z-shaped cross-sections, thin-walled H-shaped cross-sections (either hot-rolled or welded) have higher flexural stiffness and better bi-axial bending performance, and thus are increasingly being used as purlins bridging long spans. In practical engineering applications, H-section purlins are normally connected to the main truss by bolting the purlin web to a connector that is welded onto the top surface of the main truss, as shown in Fig. 1. The connector can be either an angle cleat (Fig. 1a) or a stiffened fin plate (Fig. 1b), of which the latter has greater lateral flexural resistance and also enables convenient adjustment of the vertical position of the purlin, facilitating the engineer to create freeform surfaces of the roof, and thus is usually preferred. Therefore, this paper specifically investigates the behaviour of bolted fin-plate purlin connections.

In terms of constructional details and the load-transferring mechanism, the investigated fin-plate purlin connection is very similar to the fin-plate beam-to-column connection, the progressive collapse resistance of which has already been examined in [11]. However, purlin connections are usually designed with a combination of non-preloaded bearing-type bolts and bolt holes with a comparatively larger clearance, which makes the slip of bolts a prominent phenomenon in the context of resisting progressive collapse. This constitutes a significant difference from the beam-to-column connections. In actuality, under a column (or main truss) removal scenario, the connections are subjected to internal forces that are beyond their design loads. Thus, even if a connection adopts slip-resistant bolts, on most occasions the slip of bolts is still inevitable, as observed in the tests reported in [11]. The bolt-slip behaviour in a connection postpones the activation of the catenary action, a major collapse-resisting mechanism, thereby affecting the overall bridging capacity provided by the purlins, which however was paid insufficient attention.

This study investigates the performance of the bolted fin-plate purlin connections under a main truss-removal scenario. Eight specimens with varied connection details are tested, through which the collapse-resisting mechanisms are assessed, as are the failure modes of the purlin connections. As will be shown in the tests, in different specimens the vertical displacements at which catenary action is activated show considerable difference, indicating the presence of different bolt-slip behaviour and its significant influence on the connection resistance. Furthermore, a theoretical model is developed to predict the behaviour of the purlin-to-connection assembly under a main truss-removal scenario, and is validated against the experimental results.

2. Test specimens and setup

2.1 Test specimens

Conventionally, a progressive collapse test of a beam-to-column connection takes the connection above the removed column as the experimental object. In this experimental programme, however, the purlin connection adjacent to the removed main truss (Joint A in Fig. 2), instead of the purlin connection right above the removed main truss (Joint B in Fig. 2), is to be examined. This choice is made because: a) the deformation of the bolted fin-plate connection concentrates on the bolts, the purlin web and the fin plate around and between the bolt holes, the locations of which are symmetric relative to the horizontal axis passing through the centre of the bolt group, and therefore, seeing Joint A and Joint B are subjected to antisymmetric internal forces and deformations after the removal of the main truss, they behave anti-symmetrically, such that the behaviour of one joint can be evaluated through the investigation on the other joint; and b) for certain connection configurations, e.g., a wide top chord of the main truss combined with a small gap between the bottom flange of the purlin and the top chord of the main truss, the purlin may come into contact with the main truss at Joint A, which can complicate the connection behaviour and make Joint A more critical, as schematically illustrated in Fig. 2.

The test specimens were designed as a symmetric "purlin-to-connection-to-purlin" assembly being loaded at the connections, the equivalent of which in a beam-to-column connection test, i.e., "beam-to-connection-to-beam" assembly, has been widely adopted in experimental investigations [11-14]. In addition, because the testing facilities preferred convenient application of a downward load, the test specimens were designed to be rotated 180 degrees in the vertical plane, as shown in Fig. 2. This does not alter the internal forces at the purlin connection because the dead load of the purlins was negligible compared to the applied load. Therefore, as shown in Fig. 2, in the case of presence of contact between the main truss and the purlin, the test specimens represent Joint A, while in the case of no contact, the test specimens can also represent Joint B without any need for translation of experimental results.

After the removal of a main truss, the inflection points are assumed to be located at the middle of the purlin span. Therefore, the specimen was pinned at both ends, as shown in Fig. 3, and the length between the connection and each end was equal to half of the span between the main trusses. Eight specimens were designed and tested, among which Specimen S1 was considered as the baseline model, and the other specimens featured differences in height of bolt group, location of centre of bolt group, gap between purlin and main truss, bolt grade, bolt diameter, number of bolts, and preloading force, as listed in Table 1. In Specimen S5, the gap between the purlin and the main truss (modelled as a loading column in the test) was only 5 mm, and the previously mentioned purlin-to-main truss contact could be anticipated and thus investigated.

In all specimens, the purlins featured the same radio-frequency-welded thin-walled H-section, H300x150x4.5x6, and the fin plates had the same thickness of 6 mm. Table 2 shows the material properties of the purlins and the fin plates, which were obtained from coupon tests. The bolt holes in the purlin web and in the fin plate were designed with a 2-mm clearance, i.e., the diameter of each bolt hole was 2 mm larger than the nominal diameter of the bolt, which is in accordance with the allowable maximum size of standard bolt holes in AISC 360 [15]. Moreover, although the bolts were designed as non-preloaded bearing-type bolts, the bolt installation process using a wrench automatically generated preloading forces in the bolts. The preloading force was evaluated based on the wrench torque, and was found to be about 20 kN for all specimens except for Specimen S7, in which the preloading force was increased to be about 30 kN.

2.2 Test setup

Figure 4 presents an overview of the test setup. Both ends of a specimen were pinned-connected to the horizontal supports, and the vertical load was applied through a loading column using a hydraulic jack that was supported by a loading reaction frame. The horizontal supports and the loading reaction frame were stiff enough and were firmly attached to the strong floor to resist any noticeable deformation. A lateral brace constructed with a vertical sliding support was adopted to make sure that the applied load remained vertical during entire loading process. Similar sliding support can also be found in the tests reported in [12]. The hydraulic jack had a travel distance of 500 mm which was sufficient for this experimental programme. The displacement rate was set as 2 mm/sec.

2.3 Instrumentation

All tests were instrumented as illustrated in Fig. 5. Ten displacement transducers (D1 to D10 in Fig. 5) were arranged on the top surface of the purlins to measure the deflection of the specimen. Another four displacement transducers (D11 to D14 in Fig. 5) were also arranged to monitor any possible movement of the pin support rollers at both specimen ends.

Strain gauges were arranged on three cross-sections along the length of each purlin (L1 to L3, and R1 to R3). At each selected cross-section, seven or seventeen strain gauges were arranged, as shown in Fig. 5.

The strain measurements were used to calculate the internal forces at these cross-sections, and then to calculate the load resistance provided by the specimen.

3. Test results

3.1 General behaviour and failure modes

Figure 6(a) shows the vertical load-displacement response of Specimen S1, where the displacement was taken as the average of the displacements measured by displacement transducers D1 and D2. The applied load increased linearly until the displacement reached 3 mm, producing a very short initial linear range on the load-displacement curve. The vertical deflection at this stage was too small to generate catenary action in the specimen, such that the vertical load resistance was derived from the flexural resistance of the connection. The flexural resistance resulted from the force couple of the static friction forces at the bolts, which were limited in magnitude due to the small preloading forces, and were soon overcome, leading to slip deformation at the bolts, as marked by Point "A" in Fig. 6(a). Static friction turned to kinetic friction, which was largely constant in value, and thus the flexural resistance remained nearly constant as slip deformation progressed, as demonstrated by the nearly horizontal plateau in the load-displacement curve between Point "A" and Point "B". Afterwards, the bottom bolt began to bear on the bolt holes in the purlin web and in the fin plate along the purlin length, and thus catenary action was activated considering the specimen had already undergone significant deflection. When the displacement reached 228 mm, i.e., Point "B(R)" on the load-displacement curve, the bottom bolt on the right-hand-side (RHS) purlin fractured, causing a steep drop in vertical load from 12.9 kN to 5.4 kN. This was then followed by the rapid recovery of the vertical load to another peak load of 11.3 kN at a displacement of 260 mm, Point "T(R)" on the load-displacement curve, when the top bolt on the RHS purlin fractured as well, resulting in the total loss of resistance. Therefore, in general, the Specimen S1 purlin connection failed in a failure mode marked by the fracture of bolts in shear. Photos showing the key components at the two peak loads can be found in Fig. 6(b). It is observed that the bolt holes on the purlin web experienced noticeable plastic elongation approximately in the lengthwise direction of the purlin, while the bolt holes on the fin plate underwent smaller plastic deformation.

In Specimens S2 and S3, the height of bolt group was increased to 150 mm. In addition, in Specimen S3, on each side of the connection, four grade 4.8 bolts were adopted to replace the two grade 8.8 bolts. Seeing the total shear strength of the four grade 4.8 bolts is the same as that of the two grade 8.8 bolts, Specimens S2 and S3 are collectively compared with Specimen S1 in Fig. 7(a). At the initial stage of loading, both specimens showed a linear flexural response similar to Specimen S1. However, different limits were observed for the initial linear ranges, with Specimens S3 and S1 having the largest and the smallest limits, respectively. This is readily understandable considering the force couple of the static friction forces at the bolts was affected by both the height of bolt group and the number of bolts. From the initial linear range onwards, each of Specimens S2 and S3 had a near plateau that was less apparent and also much shorter than that of Specimen S1. The reason for the different plateau lengths can be found in Section 4.1, in which a theoretical model is developed to characterise the bolt-slip behaviour. For both specimens, the near plateau stage was followed by a rapid increase in the vertical load as a result of catenary action. Specimen S2 reached the first peak load of 9.75 kN at a displacement of 155 mm when the RHS bottom bolt fractured in shear. Afterwards, the specimen regained its vertical resistance to 8.0 kN at a displacement of 234 mm, which was interrupted by the fracture of the left-hand-side (LHS) bottom bolt. The latter fracture was unexpected because normally the first failure in a connection propagates on the same side of the connection instead of on the opposite side. Specimen S2 reached its final and the largest peak load of 9.75 kN at a displacement of 314 mm. At this time, the RHS top bolt fractured in shear. Specimen S3 failed as a result of the progressive failure of the four bolts on the RHS side, leading to four peak loads on the vertical load-displacement curve. The premature first peak load was only 4.9 kN, while the ultimate resistance of the specimen was reached at the third peak load of 9.5 kN, which was close to that of Specimen S2. The above description of the experimental phenomena is depicted in Fig. 7(b).

Specimens S4 and S5 were designed to have the centres of the bolt groups moved towards the loading column by 45 mm. In specimen S5, the gap between the purlin flange and the loading column was further decreased by 25 mm, to only 5 mm. Specimen S4 performed very similarly to Specimen S1 in terms of both the vertical load-displacement response and the failure mode, as shown in Fig. 8, except that in Specimen S4 the fractured bolts were on the LHS rather than on the RHS as in Specimen S1, which is unsurprising seeing a symmetric specimen can fail on either side under symmetric loading. In addition, at the later stage of loading, Specimen S4 had slightly lower stiffness and larger deformation. The ultimate resistance was about 12.5 kN, which was reached at a displacement of 240 mm. In Specimen S5, the expected contact between the purlin flange and the loading column occurred at a displacement of 31 mm, curtailing the slip of bolts and the plateau on the load-displacement curve, as shown in Fig. 8. From then onwards, the vertical load increased rapidly and reached an ultimate value of 13.0 kN at a displacement of only 157 mm. Compared to Specimens S1 and S4, the purlin-to-loading column contact in Specimen S5 did not affect the ultimate resistance, but effectively shifted the vertical load-displacement curve leftwards.

Specimens S6, S7 and S8 featured different properties of the bolts. In Specimen S6, both bolt grade and bolt size were changed, from grade 8.8 M12 bolts in Specimen S1 to grade 4.8 M18 bolts, but the shear strength of a single bolt remained approximately unchanged, with the latter being slightly larger by 13%. As a whole, Specimen S6 performed similarly to Specimen S1, but the plateau on the load-displacement curve was shorter by a small margin of about 20 mm, thereby shifting the later part of the curve leftwards by this margin, as shown in Fig. 9 (a). The ultimate resistance was slightly larger than that of Specimen S1, i.e., 13.9 kN vs. 13.2 kN, which was most likely due to the larger bolt shear strength in Specimen S6. In Specimen S7, all bolts were installed with the larger preloading force of 30 kN, 10 kN larger than the bolt preloading force used for other specimens including Specimen S1. This resulted in a greater initial flexural resistance for the specimen, as demonstrated by the higher plateau on the force-displacement curve, as shown in Fig. 9(a). The length of the plateau was shortened by about 20 mm, but the ultimate resistance of the specimen was not altered, which was 13.1 kN reached at a displacement of 202 mm.

Specimen S8 replaced the grade 8.8 M12 bolts used for Specimen S1 with larger bolts, i.e., grade 8.8 M18 bolts. The larger bolts did not alter the initial linear response of the specimen, but shortened the bolt slip-induced plateau on the vertical load-displacement curve, as shown in Fig. 10 (a). The enlarged bolt size increased the bolt shear strength to a value that was more than twice the bolt shear strength in Specimen S1, and is also greater than both the purlin-to-bolt bearing strength and the fin plate-to-bolt bearing strength. Therefore, under the growing axial force developed in each purlin, remarkable bearing plastic deformation was observed between the bolt holes and the end of the purlin web, as depicted by Stage "A" in Fig. 10. On the vertical load-displacement curve, there are several points where the applied load transiently unloaded by a very small amount and instantaneously recovered, forming a series of fluctuations on the curve. This was generated by the deformation of the washers and their interaction with the bolt heads and the nuts during the rotation of bolts, as shown in Fig. 10. The significant plasticity around the bolt holes subsequently led to a transverse crack in the web of the purlin at a displacement of 400 mm, at which the ultimate resistance of 61.1 kN was reached. The crack initiated at the upper edge of the RHS bottom bolt hole and immediately propagated through the net-section to the top bolt hole, forming a through crack between the two bolt holes, as depicted by Stage "B" in Fig. 10. The formation of the transverse crack halved the resistance to 28.2 kN, which then recovered slightly to 29.8 kN when a longitudinal crack formed between the RHS bottom bolt hole and the end section of the purlin web, marking the final failure of the connection, as depicted by Stage "C" in Fig. 10. The failure mode of Specimen S8 was characterised by bolt bearing failure combined with net-section tensile failure, and was completely different from that of the previous seven specimens.

A summary of the test results is provided in Table 3, including the failure mode, the resistance and vertical displacement at the first peak load, as well as the ultimate resistance and the corresponding vertical displacement. It is observed that all specimens except for Specimens S2 and S3 reached the ultimate resistance at the first peak load. Moreover, although different specimens had an identical span, the vertical displacements required to activate the catenary action were different because of the different bolt-slip behaviours caused by the different connection details. For each specimen, the bolt slip-induced vertical displacement is also provided in Table 3, which is taken as the displacement corresponding to the commencement of the rapid load increase.

3.2 Resistance mechanisms

It is well known that flexural action and catenary action are the two major collapse-resisting mechanisms for frame structures subjected to a sudden column loss. In this section, to further investigate the collapse resisting mechanisms possessed by the purlin connection, the axial force and the bending moment being developed in each purlin are calculated, as are the vertical resistances respectively contributed by the flexural action and the catenary action. All recorded strains were far smaller than the strain to cause the initial yielding of the material, indicating that the purlins behaved in the elastic range during the entire loading process. Therefore, the internal forces in a purlin can be calculated based on the strain measurements at any cross-section. Sections L2 and R2 were used in this study.

At Sections L2 and R2, plane cross-sections could be assumed to remain plane under combined bending and axial tension, and therefore, the axial force, N, and the bending moment, M, can be calculated by Eq. (1) and Eq. (2), respectively.

$$N = EA \cdot \bar{\varepsilon} \tag{1}$$

$$M = EI \cdot \frac{\varepsilon_{\mathrm{t}} - \varepsilon_{\mathrm{b}}}{h} \tag{2}$$

where E is the elastic modulus; A is the section area of the purlin; I is the second moment of area of the purlin; ε_{t} and ε_{b} are respectivley the axial strain at the top and the bottom flanges, and are calculated by averaging the strain measurements on the top and the bottom flanges, respectively; $\bar{\varepsilon}$ is the axial strain of the section, which can be calculated by averaging the strains measured at evenly and symmetrically spaced locations along the height of the purlin, i.e., taking an average of ε_{t} , ε_{b} and all strains measured on the purlin web; and h is the height of purlin.

Further, the recorded displacements along the purlin length suggested that the purlins roughly remained straight during the entire loading process, which is consistent with many other beam-to-column connection tests under the column removal scenario [12]. Therefore, the shear force in the purlin at Section L2 or R2 can be calculated by:

$$V = \frac{M}{\sqrt{l^2 + \delta^2}} \tag{3}$$

where l is the distance from the pin support to Sections L2 or R2, and δ is the deflection at the section.

The vertical resistance of the specimen that was contributed by the flexural action, F_f, and by the catenary action, F_c, can thus be determined by employing Eq. (4) and Eq. (5), respectively.

$$F_\mathrm{f} = V_\mathrm{L2}\cos\theta_\mathrm{L2} + V_\mathrm{R2}\cos\theta_\mathrm{R2} \tag{4}$$

$$F_\mathrm{c} = N_\mathrm{L2}\sin\theta_\mathrm{L2} + N_\mathrm{R2}\sin\theta_\mathrm{R2} \tag{5}$$

where V_L2, N_L2 and θ_L2 are the shear force, the axial force and the rotation of Section L2, respectively; V_R2, N_R2 and θ_R2 are the shear force, the axial force and the rotation of Section R2, respectively. The rotation of a section, θ, is evaluated by $\theta = \tan^{-1}(\delta/l)$. Finally, the total vertical resistance provided by the specimen, F, combines F_f and F_c, i.e.:

$$F = F_\mathrm{f} + F_\mathrm{c} \tag{6}$$

Figure 11 shows the axial force and bending moment developed in Section L2 of Specimen S1. As soon as the test started, the bending moment increased linearly with the deflection of the specimen. After the bolt began to slip at a vertical displacement of 3 mm, the bending moment went through a stage of very slow increase, denoted as the "bolt slip" stage in Fig. 11. During this stage, until 86 mm, the axial force remained almost zero. Between 86 mm and 145 mm, the axial tension increased slowly to 6.57 kN, indicating that certain degree of catenary action was developing. However, this stage is also regarded as the bolt-slip stage because, as will be explained later in Section 4.1, during the dynamic process of bolt slip there was always factual contact between the bolt shaft and the bolt holes, resulting in the slow increase in axial tension force in the purlin.

The slip of bolts would stop only when the bottom bolt shafts and bolt holes had built effective contact along the longitudinal direction of the purlin, which occurred at about 145 mm in the case of Specimen S1, leading to the rapid increase of axial tension. Therefore, the specimen behaviour after 145 mm is regarded as the "catenary action" range, as illustrated in Fig. 11. The bending moment during this range generally remained at around the same level as the flexural action range, experiencing two temporary decreases as a result of the suddenly growing contribution of the catenary action in carrying the vertical load. The fracture of a bottom bolt at the displacement of 229 mm terminated the fast increase in axial tension, causing a drastic decrease of both the axial force and the bending moment. There was even a transient period when the bending moment reversed direction. As the displacement kept increasing, the axial force started to recover until the final failure of the connection (after the RHS bottom bolt fractured, the bending moment in the LHS purlin was able to recover somewhat).

In summary, the bolted fin-plate purlin connection investigated in this study only allowed very limited bending moment to develop in the purlin. The maximum value of the bending moment was 1.16 kN·m, which only generated a bending stress of 3.64 MPa at the outer fibre of the purlin flange. The significant deflection generated a fairly large axial tension force in the purlin with a maximum value of 80.2 kN, resulting in an axial stress of 25.9 MPa in the purlin, which is much larger than the maximum bending stress. However, seeing the purlin material had a yield stress of 300 MPa, the purlin behaved well within the elastic range under the combined action of axial tension and bending.

Having obtained the internal forces in the purlin, the contribution of the flexural action and the catenary action in providing the vertical resistance can be assessed, as shown in Fig. 12. The flexural action accounted for almost all the resistance in the early flexural-action range up until the displacement of 86 mm, when the catenary action started to have a role, corresponding to the gradually growing axial tension as shown in Fig. 11. At the displacement of 145 mm, the catenary action equalled the flexural action with respect to providing vertical resistance. Henceforth, the resistance contributed by the catenary action increased rapidly and accounted for over 90% of the total resistance, as shown in Fig. 12. Therefore, for the purlin connection investigated in this study, under a main truss-removal scenario, the vertical load resistance depends primarily on the development of an effective catenary action. In addition, the total resistance calculated by Eq. (6) was in close agreement with the applied load over the entire loading process, demonstrating that the test was well organised and performed, and the experimental results were accurately recorded.

With respect to the development of flexural action and catenary action, and their contribution to the total vertical resistance, other specimens behaved similarly to Specimen S1. Specimens S3 and S8 are chosen as examples herein for further elaboration, because Specimen S3 had four bolts on each side of the connection, and thus was able to develop greater flexural action and present a more pronounced progressive connection failure, while Specimen S8 had a failure mode different from all the other specimens. As shown in Fig. 13(a), although the connection details allowed Specimen S3 to develop greater bending moment, catenary action still contributed to over 70% of the total resistance in the catenary-action range, and contributed to about 95% of the total resistance when the specimen reached its first peak load. In Specimen S8, the catenary action provided all the vertical resistance after its full development, as demonstrated in Fig. 13(b).

Several conclusions can be drawn based on the above observations. Firstly, the response of the purlin can be divided into two distinct ranges, i.e., the flexural action range and the catenary action range, the transition between which is marked by the end of bolt slip. Secondly, flexural action and catenary action contribute to the major vertical resistance in the flexural range and the catenary range, respectively. Thirdly, the ultimate vertical resistance is controlled by the resistance of the catenary action.

3.3 Comparison and discussion

From the perspective of preventing progressive collapse, Specimens S2 and S3 showed inferior performance to Specimen S1. Firstly, the two specimens had smaller ultimate resistances than Specimen S1, by about 25%. Secondly, both specimens experienced much earlier first failure in the connection, i.e., the displacements corresponding to the first peak loads of Specimens S2 and S3 were only 38% and 72% of that of Specimen S1, respectively. Thirdly, overall, the ductility of the two specimens were not improved. Comparing to Specimen S1, Specimen S3 had a smaller ultimate displacement. As for Specimen S2, although it had a larger displacement when reaching the ultimate load, this was mostly because of its unusual failure mode, i.e., both bottom bolts fractured and thereby increased the deformability of the specimen. If Specimen S2 had failed on just one side, as all the other specimens did, similar ductilities would be expected for Specimens S2 and S1. Therefore, a preliminary suggestion for the design of bolted fin-plate purlin connections is to reduce the height of the bolt group. The reasons for this are multiple. Firstly, a large height of the bolt group may be beneficial to the flexural resistance of the connection, which however has very limited contribution to the overall resistance because it is the catenary action that provides the most of the vertical resistance. Secondly, a larger height of bolt group allows greater bending moment at the connection, which generates extra shear force at the bottom bolt, leading to its earlier failure. Thirdly, as will be shown later, increasing the height of bolt group reduces the bolt slip-induced vertical displacement, and thus reduces the total deflection of the assembly, impairing the development of the catenary action.

Comparing Specimen S4 to Specimen S1, it is shown that moving the vertical location of the bolt group had little influence on the performance of the purlin-to-connection assembly. However, comparison between Specimens S5 and S1 shows that, as expected, a small gap between the purlin flange and the main truss (the loading column in the test) creates contact at the early stage of loading. This helped reduce the bolt slip-induced vertical displacement, rendering earlier activation of the catenary action, but was detrimental on the other hand as it reduced the ductility of the connection. In the context of resisting progressive collapse, whether purlin-to-truss contact should be considered as an advantageous factor depends on the collapse-resisting behaviour of the initially damaged planar truss unit. If the planar truss resists progressive collapse through catenary action [7, 9], a large amount of ductility is desired from the purlin connection, while if the collapse-resisting mechanism of the damaged planar truss is the arch action [8], which is a mechanism without recourse to deflection, it is preferable to have an early development of vertical resistance.

Comparing Specimens S6 and S7 to Specimen S1, it is observed that, for a given height of bolt group, the ultimate resistance and the corresponding vertical displacement of the assembly are primarily controlled by the bolt shear strength, and depend less on the bolt size and the preloading force. However, Specimen S7 demonstrated that a higher bolt preloading force enhances the development of flexural action in the early loading stage, and therefore, is recommended for truss-removal scenarios where considerable vertical resistance is required under a small deflection.

Specimen S8 clearly demonstrated that, comparing to the bolt shear failure mode, the failure mode characterised by combined bolt bearing failure and net-section tensile failure was much more ductile, thereby significantly increasing the ductility and the ultimate resistance of the purlin connection. The ultimate resistance and the corresponding vertical displacement of Specimen S8 were 370% and 75% larger than those possessed by Specimen S1, respectively. Therefore, in the context of resisting progressive collapse, it is recommended that bolts being used have sufficient shear strength to achieve the more ductile bolt bearing failure mode. Moreover, to further improve the ultimate resistance, a larger end distance (i.e., the distance between bolt hole and purlin end) can be adopted to reduce the bearing plastic deformation, thereby postponing the initiation of the transverse crack.

4. Theoretical model

4.1 Bolt-slip model

The presence of bolt slip directly affects the activation of the catenary action as well as the total deflection of the purlin-to-connection assembly, and thus has an influence on the vertical load-displacement response. In this section, a mathematical model is developed to predict the bolt slip-induced vertical displacement of the assembly, by capturing the slip behaviour of each bolt inside its corresponding bolt hole.

It is observed that the slip of bolts is a process that the bolt-to-bolt hole contact changes direction from the vertical to the purlin length direction, and each bolt slips in a direction that is determined by the force applied on it, and is also confined by the bolt hole. When a purlin is installed by bolting to the fin plate, the dead load of the purlin generates an upward contact force on the upper edge of the bolt holes on the purlin web. Ideally, this aligns the bolt holes on the purlin web, the bolts, and the bolt holes on the fin plate in the vertical direction, as shown in Fig. 14(a), which is the starting point of the bolt slip. Then, the purlins tilt downwards in a test under the vertical load, or in a real structure following a sudden damage in the main truss. When the friction forces between the purlin web and the fin plate are overcome, to be compatible with this deformation, the top and bottom bolts start to move rightwards and leftwards, respectively, but are confined to remain within the bolt holes, as shown in Fig. 14(b). Therefore, the slip of bolts is a dynamic process, during which there is always contact between each bolt shaft and its corresponding bolt holes on the purlin web and on the fin plate. As the load increases, the bottom bolt gradually moves to a position where the bolt-to-bolt holes contact forces are acting in the longitudinal direction of the purlin. No further slip will occur once the position has been reached, as shown in Fig. 14(c).

To analytically characterise the above bolt-slip behaviour, a reference two-dimensional Cartesian coordinate system is established with its origin at the centre of the bottom bolt hole on the fin plate, its x-axis directed rightwards, and its y-axis directed upwards, as shown in Fig. 15. Then, the coordinates of the centres of the bolt holes on the fin plate are (0, 0) and (0, H), respectively, in which H is the height of the bolt group. From the previous discussion related to Fig. 14, it is known that the top (or bottom) bolt hole centre on the purlin web is always located on a circle centred at the top (or bottom) bolt hole centre on the fin plate, with the radius of this circle being equal to the actual clearance between the bolt and the bolt holes, C_1, as shown in Fig. 15. Due to random installation error, C_1 is always smaller than the design clearance, C, and is estimated to be 75% of C in this study, i.e., C_1=0.75C. Moreover, the assumed rigid-body movement of the purlin during the slip of bolts allows the assumption to be made that the distance between the centres of the two bolt holes on the purlin web remains unchanged, equal to H.

It follows that the coordinates of the top and bottom bolt holes on the purlin web, (x_T, y_T) and (x_B, y_B), respectively, can be obtained from the equations:

$$x_B^2 + y_B^2 = C_1^2 \tag{7}$$

$$x_T^2 + \left(y_T - H\right)^2 = C_1^2 \tag{8}$$

$$\left(x_T - x_B\right)^2 + \left(y_T - y_B\right)^2 = H^2 \tag{9}$$

Herein the purlin is assumed to be on the LHS of the connection, making the purlin rotate clockwise. Thus the leftward movement of the bottom bolt gives x_B a negative sign, and from Eq. (7), we get:

$$x_{\mathrm{B}} = -\sqrt{C_1^2 - y_{\mathrm{B}}^2} \tag{10}$$

Back-substitute Eq. (10) into Eq. (8) and Eq. (9), and solve x_{T} and y_{T}:

$$x_{\mathrm{T}} = \frac{\left(H^2 - C_1^2\right)\sqrt{C_1^2 - y_{\mathrm{B}}^2}}{H^2 - 2y_{\mathrm{B}}H + C_1^2} \tag{11}$$

$$y_{\mathrm{T}} = \frac{\left(H^2 - C_1^2\right)\left(H - y_{\mathrm{B}}\right)}{H^2 - 2y_{\mathrm{B}}H + C_1^2} \tag{12}$$

The length of the purlin is far greater than its height, implying that the rotational of the purlin is small. Thus the rotation of the purlin can be approximated through:

$$\alpha = \frac{x_{\mathrm{T}} - x_{\mathrm{B}}}{y_{\mathrm{T}} - y_{\mathrm{B}}} = \frac{2\left(H - y_{\mathrm{B}}\right)\sqrt{C_1^2 - y_{\mathrm{B}}^2}}{H^2 - 2Hy_{\mathrm{B}} + 2y_{\mathrm{B}}^2 - C_1^2} \tag{13}$$

Let φ be the angle between the line connecting the centres of the bottom bolt holes on the purlin web and on the fin plate, as shown in Fig. 15, the rotation of the purlin becomes:

$$\alpha = \frac{2HC_1 \cos\varphi - C_1^2 \cdot \sin 2\varphi}{H^2 - 2HC_1 \cdot \sin\varphi - C_1^2 \cdot \cos 2\varphi} \tag{14}$$

According to the previous discussion, the slip of bolts terminates when the line connecting the bottom bolt holes is in the longitudinal direction of the purlin. As the rotation of the purlin is small, it is reasonable to assume that the slip of bolts terminates at φ=0. Thus:

$$\alpha = \frac{2HC_1}{H^2 - C_1^2} \tag{15}$$

This rotation angle corresponds to a bolt slip-induced vertical displacement, d_{s}, of:

$$d_{\mathrm{s}} = \alpha \cdot L \tag{16}$$

where L is the distance between the pin support and the connection.

4.2 Flexural action range

Having obtained the bolt slip-induced vertical displacement, the vertical load-displacement response in the flexural action range can be obtained. Based on the experimental observation and discussion, two assumptions are made to simplify the calculation. Firstly, the initial stiffness of the purlin-to-connection assembly is evaluated by considering the assembly as a simply supported beam, ignoring the deformation within the connection. Secondly, the vertical resistance during the bolt-slip stage is only contributed by the flexural action, ignoring the contribution of the catenary action in the later flexural-action range.

According to the simple beam theory, the initial stiffness of the assembly is:

$$K_{\mathrm{e}} = \frac{6EI}{L^3} \tag{17}$$

The ultimate resistance provided by the flexural action, $F_{\mathrm{f\text{-}u}}$, is reached when the maximum static friction forces between the purlin web and the fin plate are overcome, and is calculated as:

$$F_{\mathrm{f\text{-}u}} = \frac{2M_{\mathrm{s}}}{L} \tag{18}$$

where M_{s} is the slip-resisting moment of a bolt group, and is equal to $F_{\mathrm{s}} \cdot H$ for a connection with only two bolts on each side of the connection, in which F_{s} is the slip resistance of a bolt for given preloading force and friction coeeficient.

Therefore, the bolt-slip plateau starts from the displacement of $F_{\mathrm{f\text{-}u}}/K_{\mathrm{e}}$, and finishes at the displacement of d_{s}.

4.3 Catenary action range

A component-based spring model is developed for determining the vertical load-displacement response of the purlin-to-connection assembly in the catenary-action range. An assumption is made herein that the vertical resistance in the catenary range is solely provided by the catenary action, which is reasonable because the flexural resistance contributes to a very small percentage of the total resistance in this range. Thus, the spring model only accounts for the axial behaviour of the purlin-to-connection assembly. Moreover, the symmetry of the assembly permits modelling only half of the assembly. Figure 16 presents the spring model developed for an assembly with two bolts on each side of the connection, i.e., all the specimens tested in this study except for Specimen 3. In this model, the axial behaviour of the purlin is modelled with an elastic spring, (p), while the bolt in shear, the purlin-to-bolt in bearing, and the fin plate-to-bolt in bearing components are modelled with bilinear springs, (bs), (pb) and (fb), respectively, in order to capture the gradual yielding and failure characteristic of these components.

Normally, the same components in the top and bottom spring series, for example, the two bolt in shear components, follow an identical force-displacement rule. This however is not true for this catenary action model, because when the catenary action starts, the previous bolt-slip behaviour has created different contact conditions for the bolts at different bolt rows, as shown in the box in Fig. 16. At the bottom bolt, pairs of longitudinal contact have already been established. At the top bolt, to establish similar pairs of contact, the purlin has to travel a distance of C_2, which is smaller than $2C_1$, the diameter of the circle forming the moving path of the bolt hole centre on the purlin web. For the sake of simplicity, but without loss of generality, C_2 is assumed to have a constant value of $\frac{2}{3}$ of the circle diameter, i.e., $C_2=\frac{4}{3}C_1=C$. Therefore, all components at the top bolt row are only activated when a displacement of C_2 is reached, as shown in Fig. 16.

Having determined the force-displacement rule for each component, using experimental data or provisions in design codes of Eurocode 3 Part 1-8 [16], the axial force-displacement (F_a-Δ_a) relationship of the spring model can be obtained by simply assembling the springs, i.e., springs in parallel are subject to an identical displacement, while springs in series are subject to an identical force. When a component fails by reaching the ultimate strength, the resistance contributed by the bolt row where the failed component belongs to is subtracted from the total resistance, and the calculation proceeds until the failure of all bolt rows.

Then, the vertical displacement d, and the vertical resistance, F, can be calculated from Eq. (19) and Eq. (20), respectively, which are based on the simplified geometrical relationship shown in Fig. 17.

$$d = \sqrt{d_s^2 + \Delta_a^2 + 2\Delta_a \sqrt{L^2 + d_s^2}} \tag{19}$$

$$F = 2F_a \cdot \frac{d}{\sqrt{d^2 + L^2}} \tag{20}$$

5. Model validation

For the purpose of validation, the above proposed theoretical model is applied to the tests reported in Sections 2 and 3, except for Specimen S5 in which contact occurred between the purlin and the loading column, creating a bolt-slip behaviour which was quite different from the theoretical model.

Seeing the bolt in shear, purlin-to-bolt in bearing and fin plate-to-bolt in bearing components all contribute to the plastic deformation, these three components are all modelled with springs with full-range bi-linear force-displacement relationships, as shown in Fig. 16. The initial stiffness, K_e, and the ultimate strength, P_u, of each component are calculated according to Eurocode 3 Part 1-8 [16], and the elastic limit strength, P_y, is estimated by using the same equations for calculation of P_u, in which however the ultimate tensile strength (f_u) is replaced with the yield stress (f_y). The plastic stiffness of a component is assumed to be a fixed percentage of the initial stiffness, which is adopted as γ=5% for all three components. This percentage value is close to that used in [17, 18]. The purlin is modelled with an elastic spring, the stiffness of which is determined as $K_e^p = EA/L$. Table 4 summarises the properties of each component.

Using the above component properties, the axial force-displacement relationship of the connection can be determined, as shown in Figure 18 in which Specimen S1 is taken as an example. Note that the forces that cause the yielding of the purlin-to-bolt in bearing component and the yielding of the fin plate-to-bolt in bearing component are very close, and therefore, for simplicity, these two components are approximated to yield under the same force of 38.1 kN.

Figure 19 shows the model predictions as well as the comparisons against the experimental results. It is observed the proposed model is capable of capturing the experimental phenomena, including the slip of bolts, the yielding and failure of components, and thus gives reasonably good predictions on the force-displacement curves, the failure modes and the failure loads. Some discrepancy is observed for Specimens S3 and S8. However, the response of Specimen S3 prior to the first failure is well captured, and the discrepancy for Specimen S8 most likely results from a less accurate force-displacement assumption for the bolt in bearing components derived from Eurocode 3. Thus, the presented model is considered adequate for the design of purlin connections against progressive collapse.

6. Conclusion

This paper presents a comprehensive investigation of the bolted fin-plate purlin connections, studying their performance under a main truss removal scenario.

Eight purlin-to-connection assemblies with varied connection details were tested. The specimens showed several common characteristics. An elastic initial response was observed, which was contributed by the flexural action of the assembly. As the flexural action grew, it generated slip-resistance demands greater than the maximum static friction forces at the bolts, leading to the slip of bolts. During this period, the flexural action remained almost unchanged and negligible catenary action developed. After effective contact was established between the bolt shaft and the bolt holes along the purlin length, catenary action was activated, leading to a rapid increase of the axial tension force, which contributed to the major vertical resistance.

Differences in response were observed in the specimens due to the varied connection details. Most importantly, different failure modes were resulted from the use of bolts with different shear strengths. If the bolt shear strength was smaller than the bolt bearing strength, the connection failed in a bolt shear failure mode. Otherwise, the connection showed a failure mode that was characterised by the bolt bearing failure combined with the net-section tensile failure. The latter failure mode provided much greater ductility and was capable of sustaining considerably greater vertical load. Meanwhile, the height and location of the bolt group, the gap between the purlin flange and the main truss, as well as the preloading force in the bolts, all influenced the performance of the purlin connection. From the standpoint of increasing the bridging capacity of the purlin, it is recommended to adopt relatively larger diameter bolts, reduce the height of the bolt group, apply higher preloading force when installing the bolts, and increase the end distance for the bolt holes.

A theoretical model is proposed to predict the behaviour of the purlin-to-connection assembly. The initial elastic response is obtained using simple beam theory and the equilibrium of moment. The bolt slip-induced vertical displacement is evaluated through a mathematical bolt-slip model, which characterises the slip of bolts inside the corresponding bolt holes. The catenary action is estimated using a spring-based model, in which the connection components, including the bolt in shear, the purlin-to-bolt in bearing, and the fin plate-to-bolt in bearing components, are modelled with bi-linear force-displacement relationships, such that the catenary model is capable of capturing the gradual yielding and failure of the connection components. Fairly good agreement is observed between the model predictions and the experimental results, in terms of both the vertical resistance-displacement curves and the failure modes, as well as the failure loads.

Acknowledgement

The work presented in this paper was funded by the National Natural Science Foundation of China through Grant No. 51678432, and by the Australian Research Council through Discovery Project Grant No. DP150104873.

References

[1] Izzuddin BA, Vlassis AG, Elghazouli AY, Nethercot DA. Progressive collapse of multi-storey buildings due to sudden column loss - Part I: Simplified assessment framework. Eng Struct 2008, 30(5): 1308–1318.

[2] Yi W, He Q, Xiao Y, Kunnath SK. Experimental study on progressive collapse-resistant behavior of reinforced concrete frame structures. ACI Struct J 2008, 105(4): 433–439.

[3] Kim J, Kim T. Assessment of progressive collapse-resisting capacity of steel moment frames. J Constr Steel Res 2009, 65(1): 169–179

[4] Zhao X, Yan S, Chen Y. Comparison of progressive collapse resistance of single-layer latticed domes under different loadings. J Constr Steel Res 2017, 129: 204-214.

[5] Xu Y, Han Q, Parke GAR, Liu Y. Experimental study and numerical simulation of the progressive collapse resistance of single-layer latticed domes. J Struct Eng 2017, 143(9): 04017121.

[6] Yan S, Zhao X, Rasmussen KJR, Zhang H. Identification of critical members for progressive collapse analysis of single-layer latticed domes. Eng Struct 2019, 188: 111-120.

[7] Zhao X, Yan S, Chen Y, Xu Z, Lu Y. Experimental study on progressive collapse-resistant behavior of planar trusses. Eng Struct 2017, 135: 104-116.

[8] Yan S, Zhao X, Lu Y. Collapse-resisting mechanisms of planar trusses following sudden member loss. J Struct Eng, 2017, 143(9): 04017114.

[9] Yan S, Zhao X, Chen Y, Xu Z, Lu Y. A new type of truss joint for prevention of progressive collapse. Eng Struct 2018, 167: 203-213.

[10] Chen Y, Zhao X, Wang L, Yan S. Progressive collapse of large span truss-beam structures induced by initial member break. IABSE Workshop on Safety, Robustness and Condition Assessment of Structures, Helsinki, Finland, 2015: 112-119.

[11] Yang B, Tan KH. Experimental tests of different types of bolted steel beam-columns joints under a central-column-removal scenario. Eng Struct 2013, 54: 112–130.

[12] Li L, Wang W, Chen Y, Lu Y. Experimental investigation of beam-to-tubular column moment connections under column removal scenario. J Constr Steel Res 2013, 88: 244–255.

[13] Gong Y. Test, modeling and design of bolted-angle connections subjected to column removal. J Constr Steel Res 2017, 139: 315–326.

[14] Liu C, Tan KH, Fung TC. Investigations of nonlinear dynamic performance of top-and-seat with web angle connections subjected to sudden columns removal. Eng Struct 2015, 99: 449–461.

[15] ANSI/AISC 360-10. Specification for structural steel buildings. American Institute of Steel Construction; 2010.

[16] CEN Comité Européen de Normalisation. 1993-1-8: Eurocode 3: design of steel structures – part 1–8: Design of joints. Brussels (Belgium): CEN; 2010.

[17] Simões Da Silva L, Santiago A, Vila Real P, Post-limit stiffness and ductility of endplate beam-to-column steel joints. Comput Struct 2002, 80: 515–531.

[18] Zhu C, Rasmussen KJR, Yan S. Generalised component model for structural steel joints. J Constr Steel Res 2019, 153: 330–342.

Figures

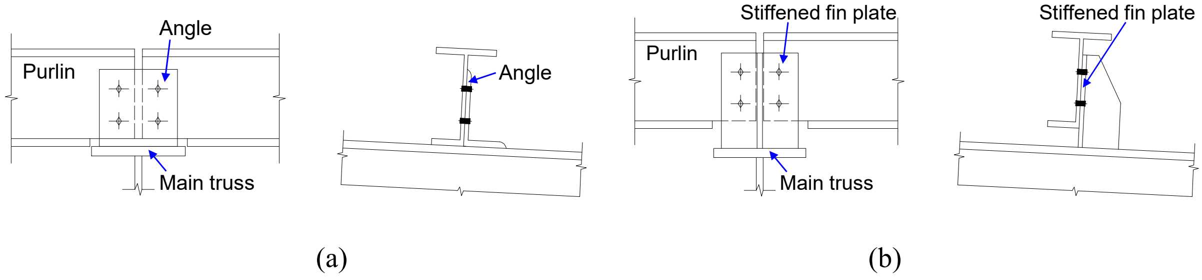

Fig. 1. Purlin connection. (a) using angle; (b) using stiffened fin plate.

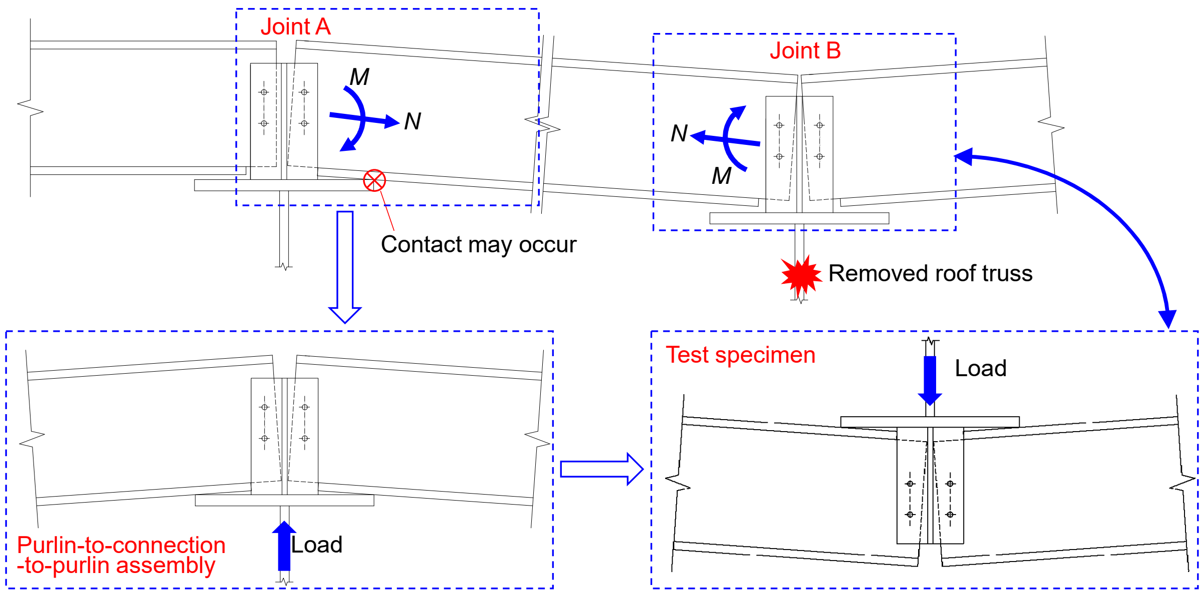

Fig. 2. Specimen design considerations.

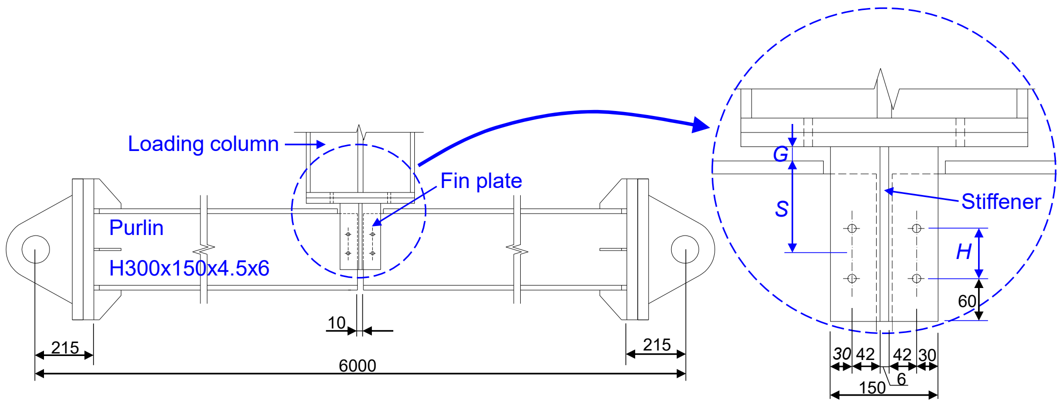

Fig. 3. Geometry of test specimens.

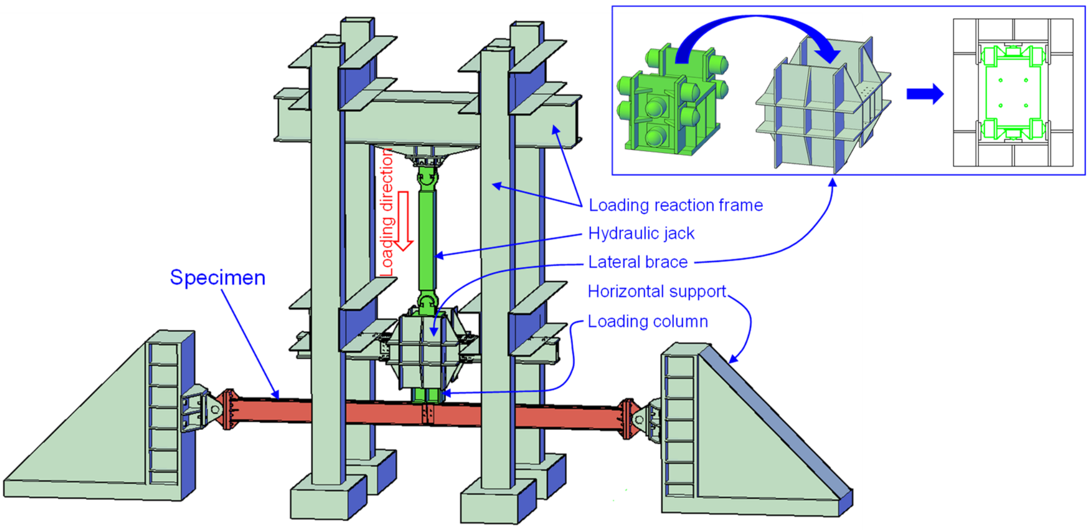

Fig. 4 Test setup.

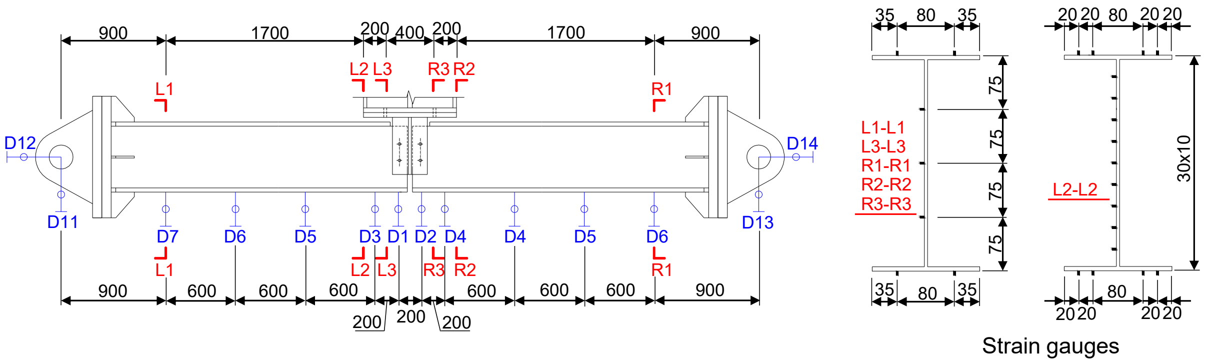

Fig.5. Experimental instrumentation arrangement.

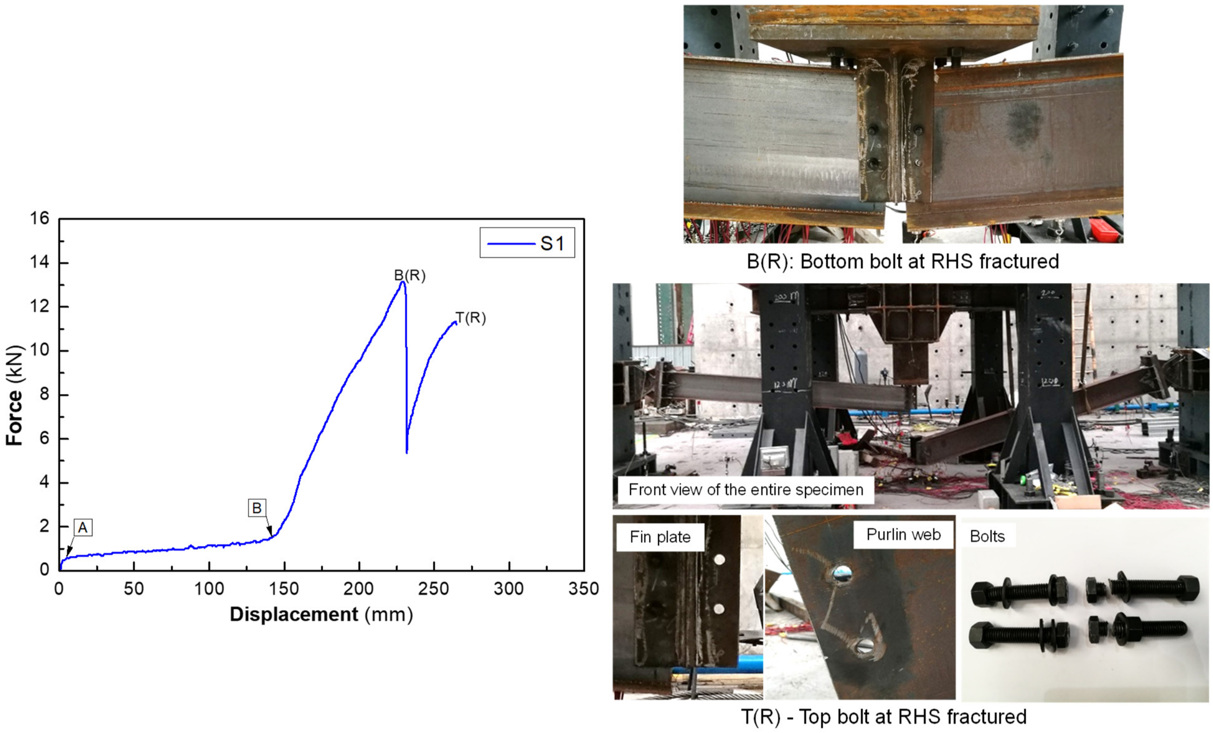

(a) (b)

Fig. 6. Behaviour of Specimen S1. (a) Vertical load-connection displacement curve; (b) experimental phenomena.

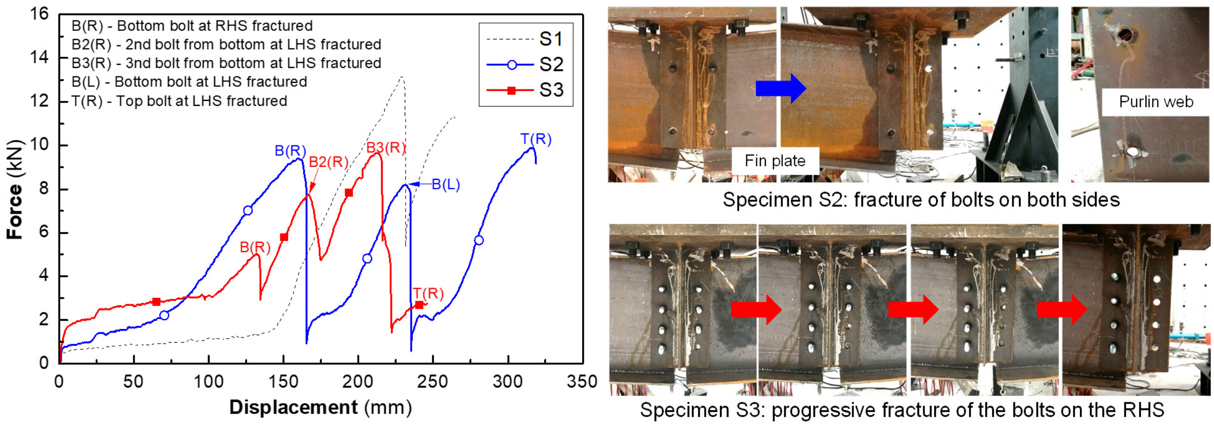

(a) (b)

Fig. 7. Behaviour of Specimens S2 and S3. (a) Vertical load-connection displacement curves; (b) experimental phenomena.

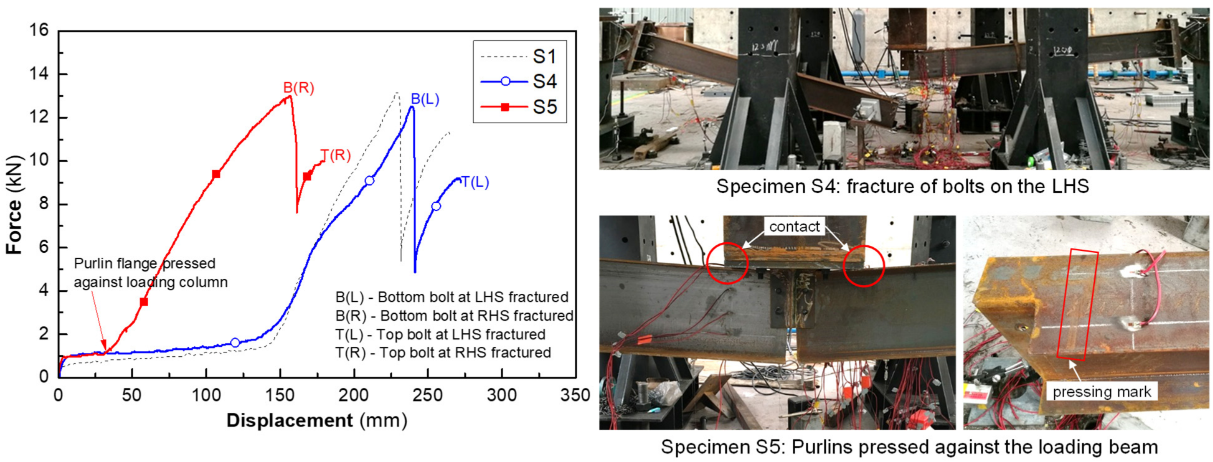

(a) (b)

Fig. 8. Behaviour of Specimens S4 and S5. (a) Vertical load-connection displacement curves; (b) experimental phenomena.

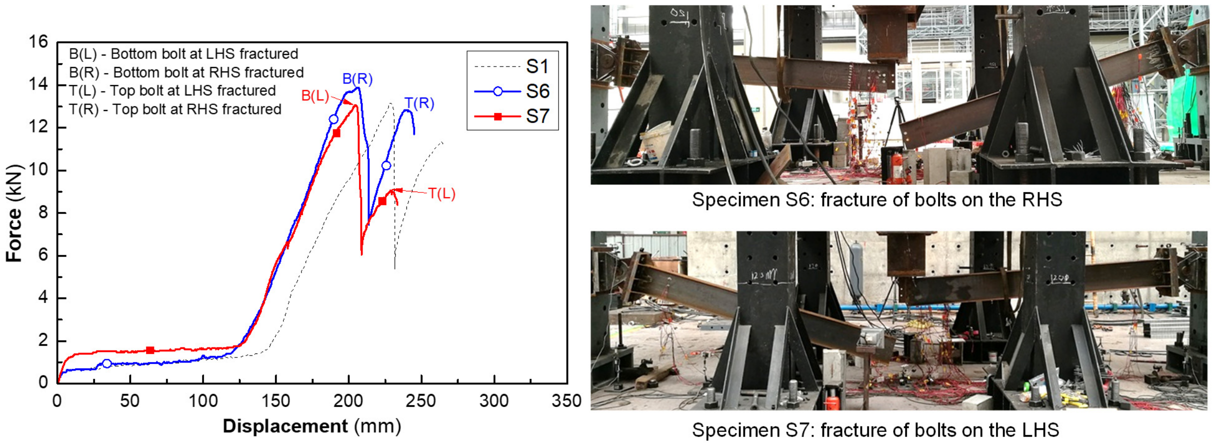

(a) (b)

Fig. 9. Behaviour of Specimens S6 and S7. (a) Vertical load-connection displacement curves; (b) experimental phenomena.

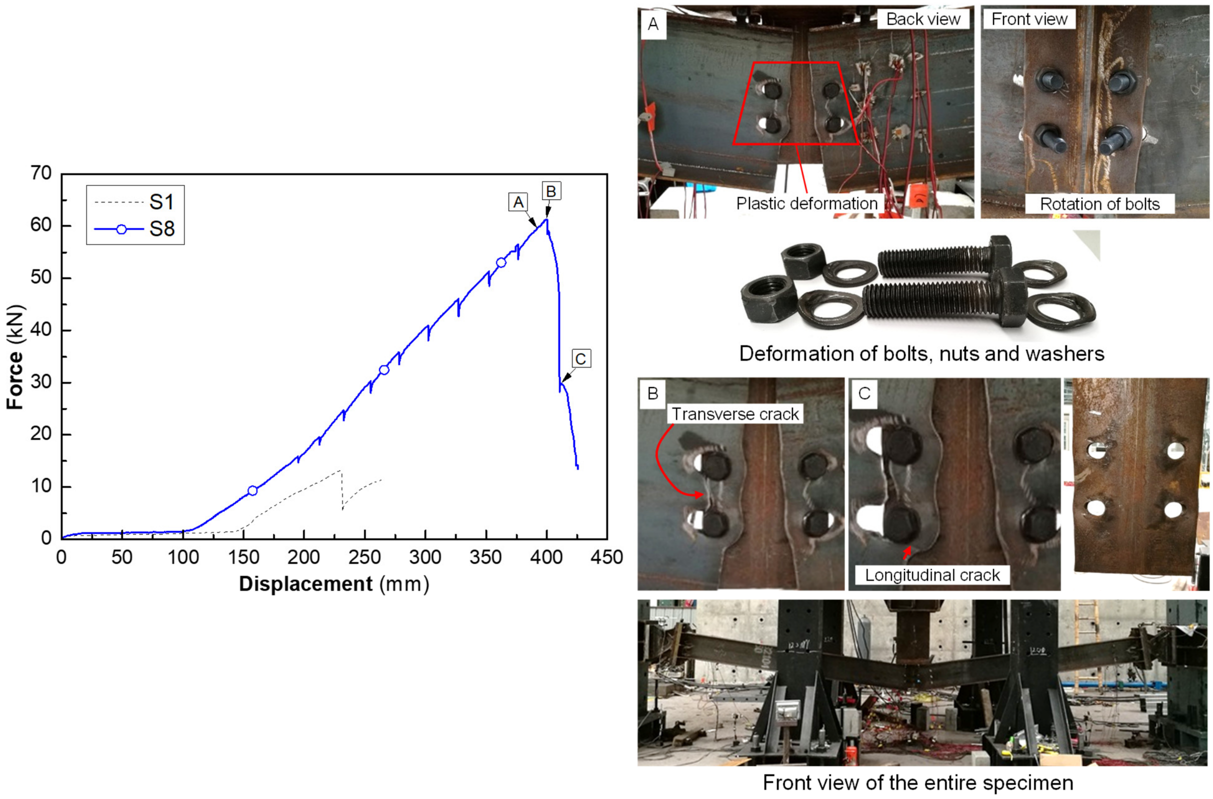

(a) (b)

Fig. 10. Behaviour of Specimens S8. (a) Vertical load-connection displacement curves; (b) experimental phenomena.

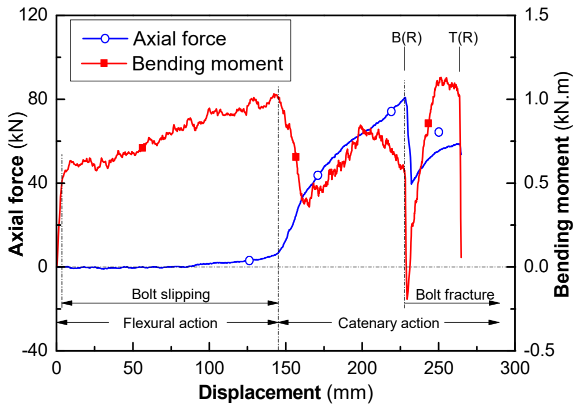

Fig. 11. Axial tension force and bending moment in Specimen S1.

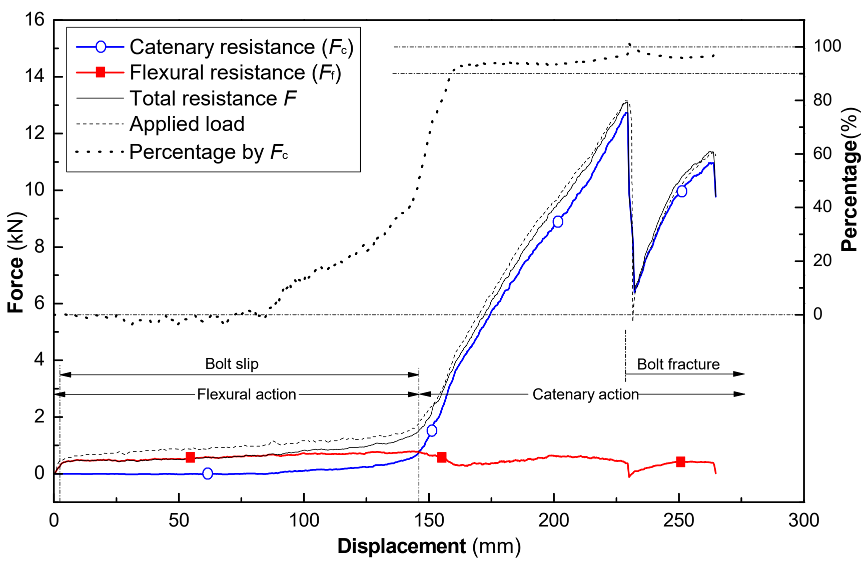

Fig. 12. Vertical resistance of Specimen S1.

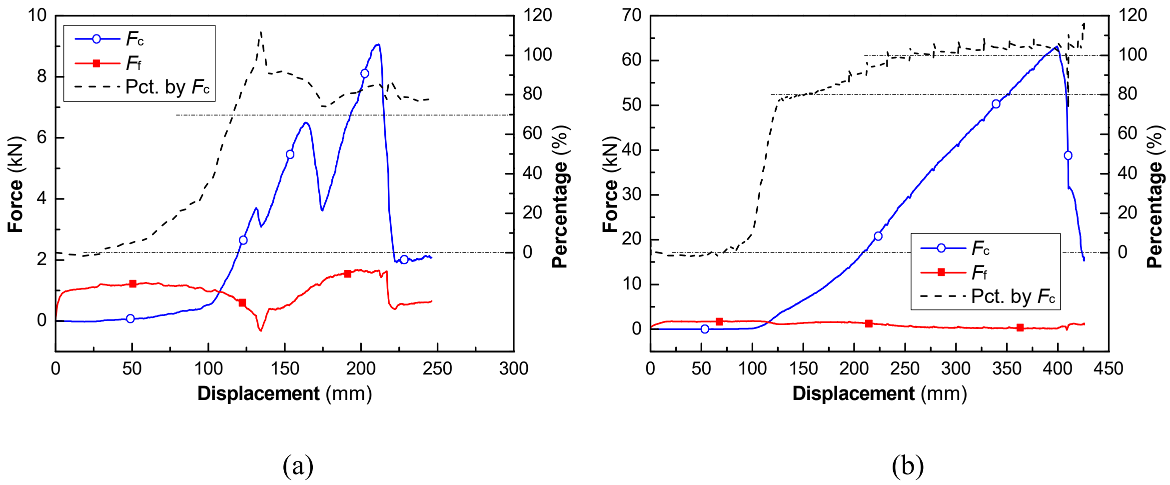

Fig. 13. Vertical resistance of specimens S3 and S8. (a) S3; (b) S8.

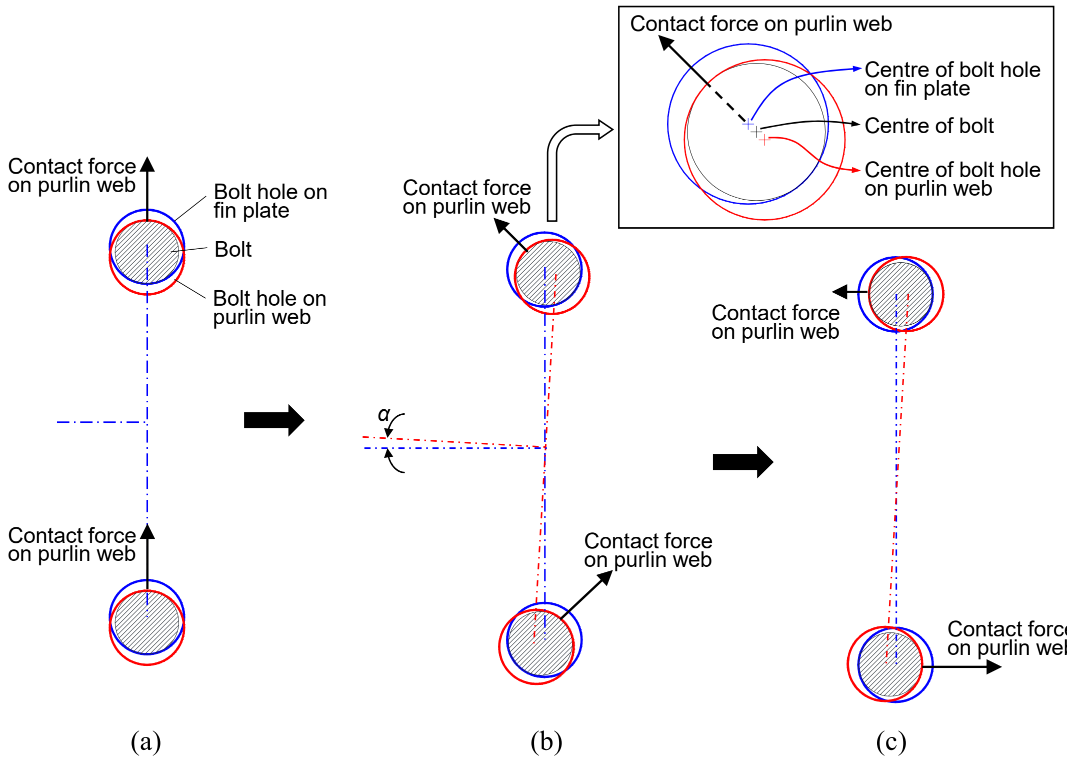

Fig. 14. Slip of bolts in bolt holes.

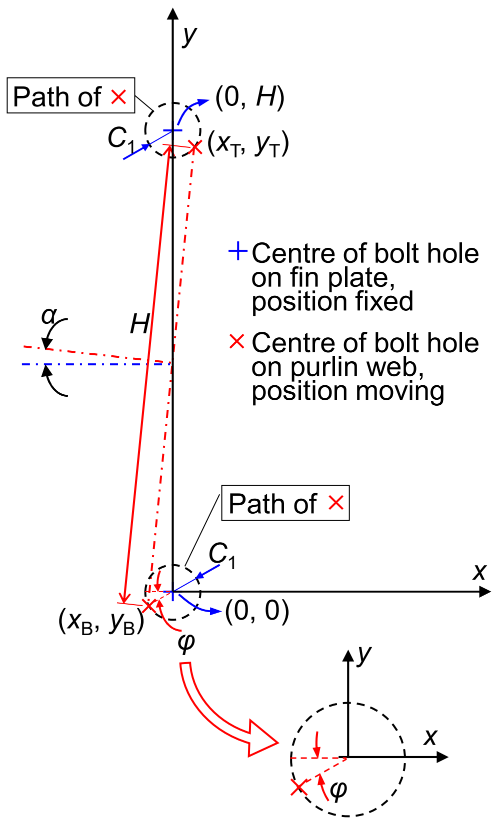

Fig. 15. Calculation model of bolt-slip behaviour.

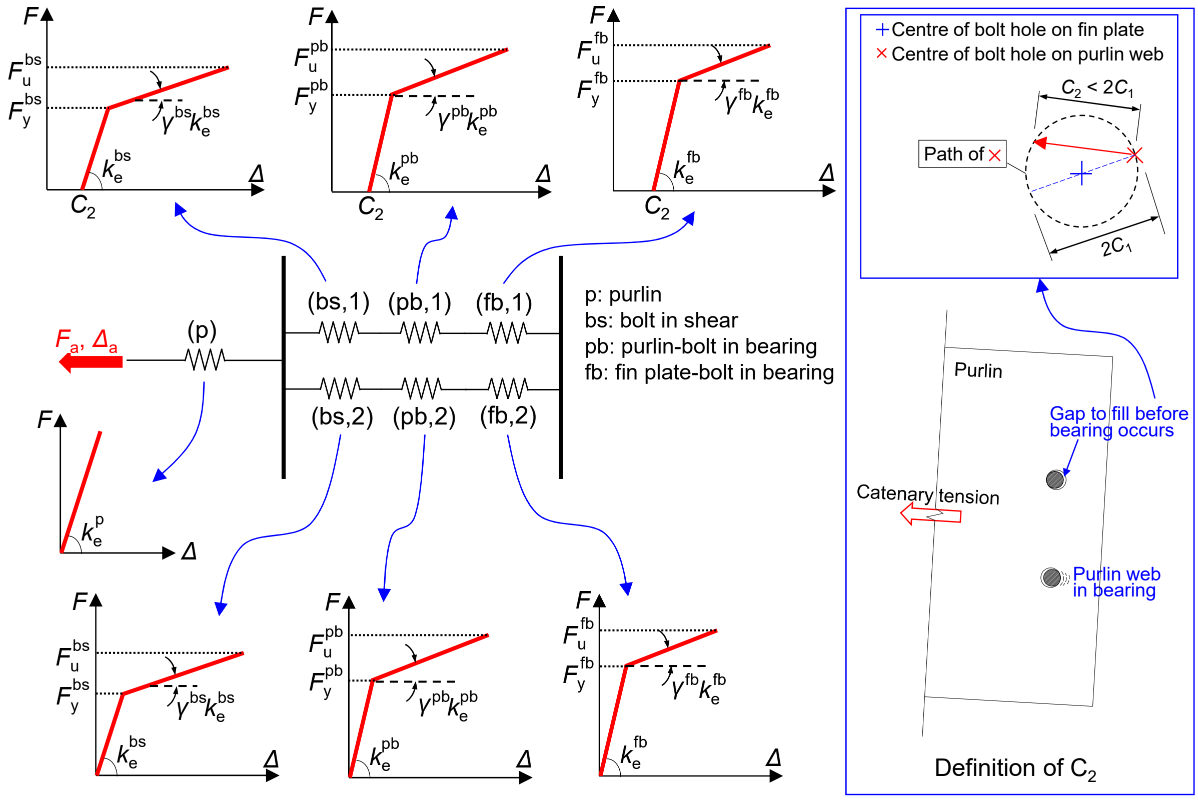

Fig. 16. Spring model for axial tension of purlin-to-connection assembly.

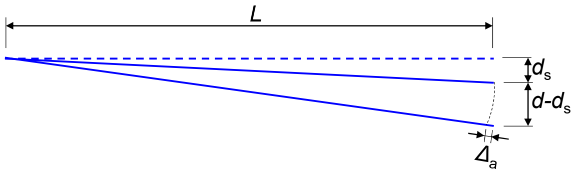

Fig. 17. Calculation of vertical displacement d.

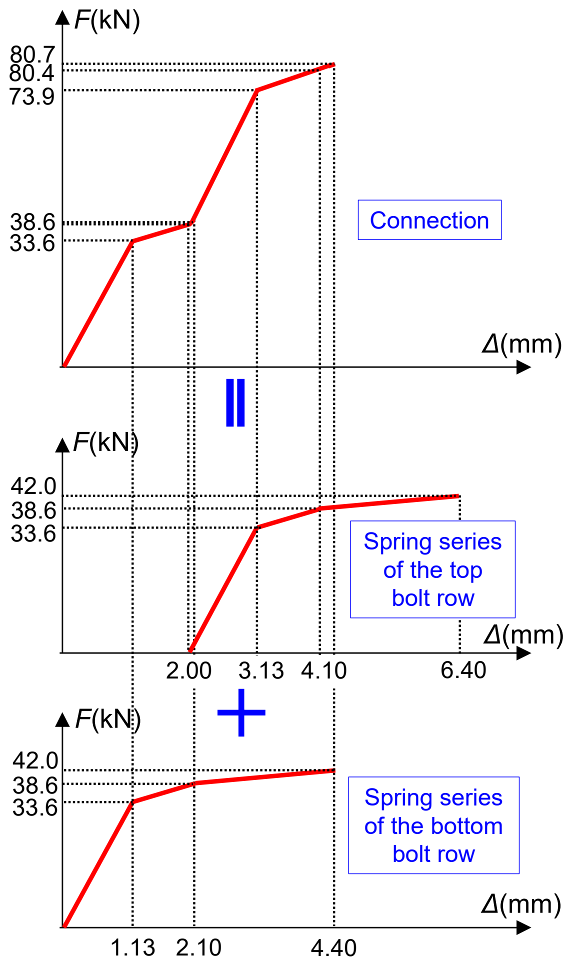

Fig. 18. Force-displacement relationship for Specimen S1 connection.

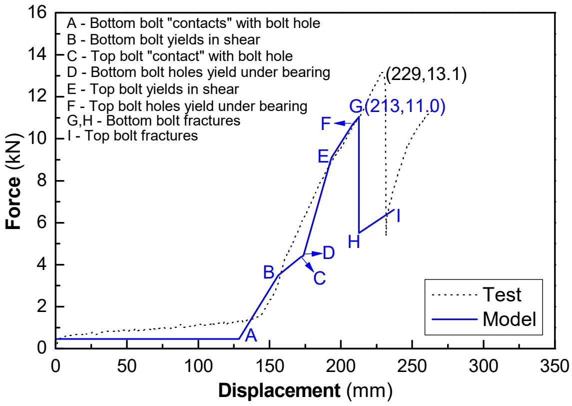
A - Bottom bolt "contacts" with bolt hole
B - Bottom bolt yields in shear
C - Top bolt "contact" with bolt hole
D - Bottom bolt holes yield under bearing
E - Top bolt yields in shear
F - Top bolt holes yield under bearing
G,H - Bottom bolt fractures
I - Top bolt fractures
(229,13.1)
G(213,11.0)
Test
Model
Force (kN)
Displacement (mm)

(a)

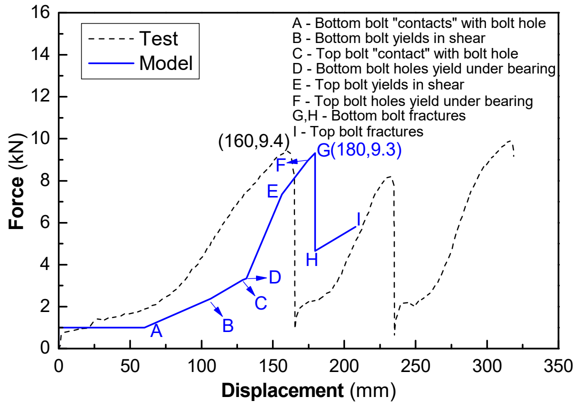
Test
Model
A - Bottom bolt "contacts" with bolt hole
B - Bottom bolt yields in shear
C - Top bolt "contact" with bolt hole
D - Bottom bolt holes yield under bearing
E - Top bolt yields in shear
F - Top bolt holes yield under bearing
G,H - Bottom bolt fractures
I - Top bolt fractures
(160,9.4)
G(180,9.3)
Force (kN)
Displacement (mm)

(b)

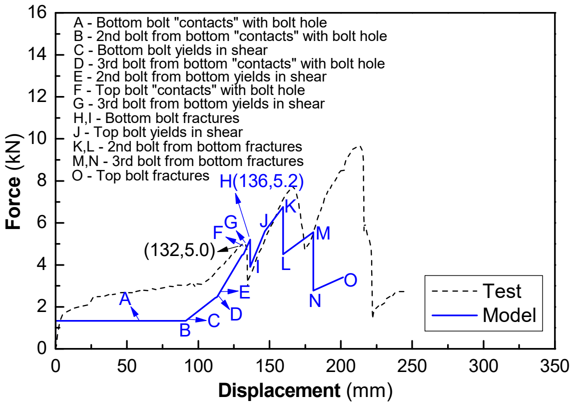
A - Bottom bolt "contacts" with bolt hole
B - 2nd bolt from bottom "contacts" with bolt hole
C - Bottom bolt yields in shear
D - 3rd bolt from bottom "contacts" with bolt hole
E - 2nd bolt from bottom yields in shear
F - Top bolt "contacts" with bolt hole
G - 3rd bolt from bottom yields in shear
H,I - Bottom bolt fractures
J - Top bolt yields in shear
K,L - 2nd bolt from bottom fractures
M,N - 3rd bolt from bottom fractures
O - Top bolt fractures
H(136,5.2)
(132,5.0)
Test
Model
Force (kN)
Displacement (mm)

(c)

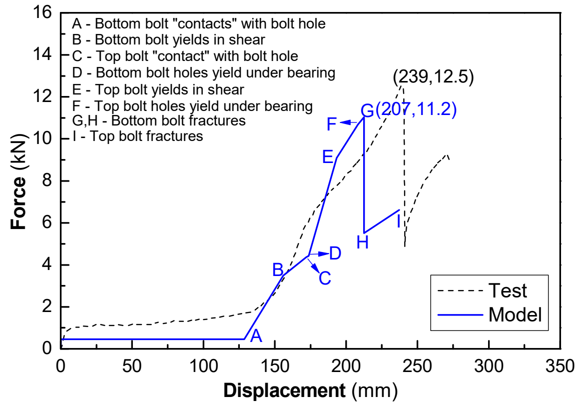
A - Bottom bolt "contacts" with bolt hole
B - Bottom bolt yields in shear
C - Top bolt "contact" with bolt hole
D - Bottom bolt holes yield under bearing
E - Top bolt yields in shear
F - Top bolt holes yield under bearing
G,H - Bottom bolt fractures
I - Top bolt fractures
(239,12.5)
G(207,11.2)
Test
Model
Force (kN)
Displacement (mm)

(d)

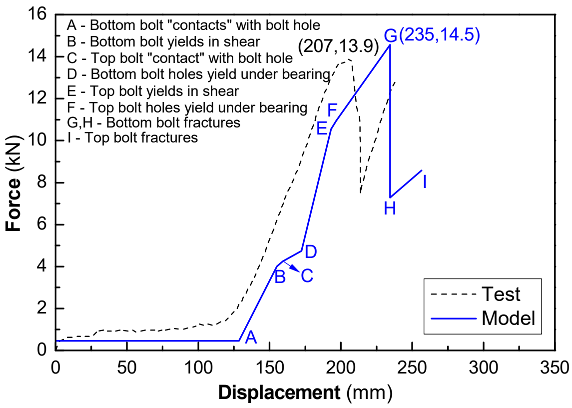
A - Bottom bolt "contacts" with bolt hole
B - Bottom bolt yields in shear
C - Top bolt "contact" with bolt hole
D - Bottom bolt holes yield under bearing
E - Top bolt yields in shear
F - Top bolt holes yield under bearing
G,H - Bottom bolt fractures
I - Top bolt fractures
(207,13.9)
G(235,14.5)
Test
Model
Force (kN)
Displacement (mm)

(e)

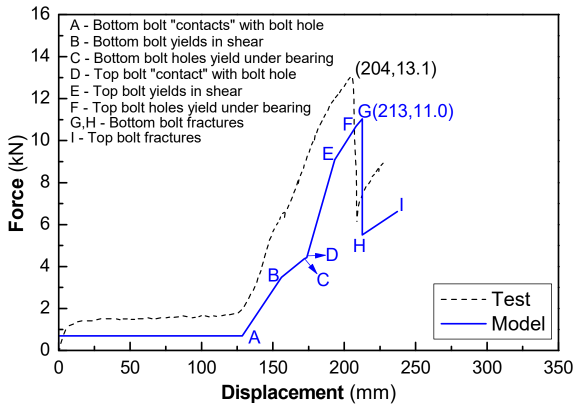
A - Bottom bolt "contacts" with bolt hole
B - Bottom bolt yields in shear
C - Bottom bolt holes yield under bearing
D - Top bolt "contact" with bolt hole
E - Top bolt yields in shear
F - Top bolt holes yield under bearing
G,H - Bottom bolt fractures
I - Top bolt fractures
(204,13.1)
G(213,11.0)
Test
Model
Force (kN)
Displacement (mm)

(f)

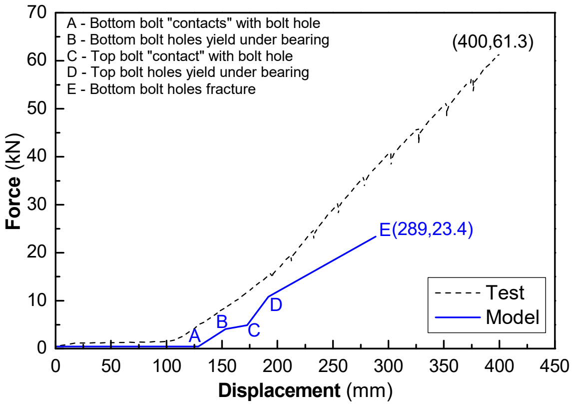

(g)

Fig. 19. Vertical force-displacement response predicted by the proposed model. (a) Specimen S1; (b) Specimen S2; (c) Specimen S3; (d) Specimen S4; (e) Specimen S6; (f) Specimen S7; (g) Specimen S8.

Tables

Table 1. General feature of specimens (refer Fig.3 for nomenclature).

Specimen	Height of bolt group H (mm)	Location of centre of bolt group S (mm)	Gap between purlin and loading column G (mm)	Bolt grade	Bolt diameter (mm)	Number of bolts	Preload (kN)
S1	**70**	**150**	**30**	**8.8**	**12**	**2**	**20**
S2	**150**	150	30	8.8	12	2	20
S3	**150**	150	30	**4.8**	12	**4**	20
S4	70	**105**	30	8.8	12	2	20
S5	70	**105**	**5**	8.8	12	2	20
S6	70	150	30	**4.8**	**18**	2	20
S7	70	150	30	8.8	12	2	**30**
S8	70	150	30	8.8	**18**	2	20

Table 2 Material properties

	Yield stress f_y (MPa)	Tensile strength f_u (MPa)	Elongation δ (%)
Purlin flange	374	472	39%
Purlin web	296	468	42%
Fin plate	300	484	46%

Table 3. Summary of experimental results.

Specimen	Failure mode	First peak Resistance (kN)	First peak Displacement (mm)	Ultimate Resistance (kN)	Ultimate Displacement (mm)	Displacement induced by bolt slip (mm)
S1	BSF	13.1	229	13.1	229	144
S2	BSF	9.40	160	9.89	316	70
S3	BSF	5.02	132	9.65	213	101
S4	BSF	12.5	239	12.5	239	136
S5	BSF	13.0	157	13.0	157	31
S6	BSF	13.9	207	13.9	207	118
S7	BSF	13.1	204	13.1	204	127
S8	BBF & NTF	61.3	400	61.3	400	106

Note: BSF – bolt shear failure; BBF – bolt bearing failure; NTF – net-section tensile failure.

Table 4. Summary of component properties.

Component		K_e (N/mm)	γ	F_y (kN)	F_u (kN)
Purlin		212,000	–	–	–
Grade 8.8 M12 bolt	Bolt in shear	120,000	0.05	33.6	42.0
	Purlin-bolt in bearing	71,100	0.05	38.1	60.2
	Fin plate-bolt in bearing	88,200	0.05	38.6	62.2
Grade 4.8 M12 bolt	Bolt in shear	60,500	0.05	17.0	21.2
	Purlin-bolt in bearing	71,100	0.05	35.9	56.7
	Fin plate-bolt in bearing	88,200	0.05	38.6	62.2
Grade 8.8 M18 bolt	Bolt in shear	269,000	0.05	76.5	95.6
	Purlin-bolt in bearing	90,000	0.05	40.0	63.2
	Fin plate-bolt in bearing	108,000	0.05	40.5	65.3
Grade 4.8 M18 bolt	Bolt in shear	136,000	0.05	38.7	48.4
	Purlin-bolt in bearing	90,000	0.05	40.0	63.2
	Fin plate-bolt in bearing	108,000	0.05	40.5	65.3